As–(Ag) sulphide veins in the Spanish Central System: further evidence for a hydrothermal event of Permian age

Tomás Martín-Crespo[a,*], Elena Vindel[b], José Angel López-García[b], Esteve Cardellach[c]

[a] *Escuela Superior de Ciencias Experimentales y Tecnología, Universidad Rey Juan Carlos, E. Departamental I, Móstoles, Madrid 28933, Spain*

[b] *Departamento de Cristalografía y Mineralogía, Facultad de Ciencias Geológicas, Universidad Complutense, Madrid 28040, Spain*

[c] *Departament de Geologia, Facultat de Ciencies, Universitat Autònoma, Bellaterra 08193, Barcelona, Spain*

Abstract

The Spanish Central System (SCS) has been subjected to repeated deformation and fluid flow events which have produced both sulphide-bearing and barren vein systems. Although several hydrothermal episodes took place between 300 and 100 Ma, fluid circulation during the Permian was especially important, giving rise to a range of different types of deposits. This study presents a multidisciplinary approach leading to the characterisation of the chemistry and age of the hydrothermal fluids that produced the As–(Ag) mineralised stockwork of Mónica mine (Bustaviejo, Madrid). Fluid inclusion data indicate the presence of two different fluids. An initial ore stage (I) formed from a low- to moderate salinity (3–8 wt.% eq. NaCl) H_2O–NaCl–CO_2–CH_4 fluid, at minimum trapping temperature of 350 ± 15 °C and 0.3 kbar. A second H_2O–NaCl fluid is found in three types of fluid inclusions: a high temperature and low salinity type (340 ± 20 °C; 0.8–3.1 wt.% eq. NaCl) also associated to ore stage I, a moderate temperature and very low salinity type (160–255 °C; 0–1.5 wt.% eq. NaCl) represented in ore stage III, and a very low temperature and hypersaline type (60–70 °C; 30–35 wt.% NaCl), unrelated to the mineralising stages and clearly postdating the previous types. ^{40}Ar–^{39}Ar dating on muscovite from the early As–Fe stage (I) has provided an age of 286 ± 4 Ma, synchronous with the late emplacement phases of La Cabrera plutonic massif (288 ± 5 Ma) and with other Permian hydrothermal events like Sn–W skarns and W–(Sn) sulphide veins. $\delta^{18}O$ of water in equilibrium with stage I quartz (5.3–7.7‰), δD of water in equilibrium with coexisting muscovite (−16.0‰ to −2.0‰), and sulphide $\delta^{34}S$ (1.5–3.6‰) values are compatible with waters that leached metamorphic rocks. The dominant mechanism of the As–(Ag) deposition was mixing and dilution processes between aqueous–carbonic and aqueous fluids for stage I (As–Fe), and nearly isobaric cooling processes for stages II (Zn–Cu–Sn) and III (Pb–Ag). The origin and hydrothermal evolution of As–(Ag) veins is comparable to other hydrothermal Permian events in the Spanish Central System.

Keywords: Fluid inclusions; Stable isotopes; Hydrothermal fluids; Permian; Spanish Central System

1. Introduction

Episodic hydrothermal events, ranging from the Variscan orogeny to the present day, have been recog-

* Corresponding author. Fax: +1-34-91-664-74-90.
E-mail address: t.martin@escet.urjc.es (T. Martín-Crespo).

nised in the Spanish Central System (SCS). Among them, those developed during the Permian age are the most widely represented, and contributed to formation of a wide range of granite- and metamorphic-hosted mineral deposits and associated hydrothermal alteration. Hydrothermal activity in the SCS was related to the most voluminous of the episodes of granitoid emplacements and to regional neoformation and/or

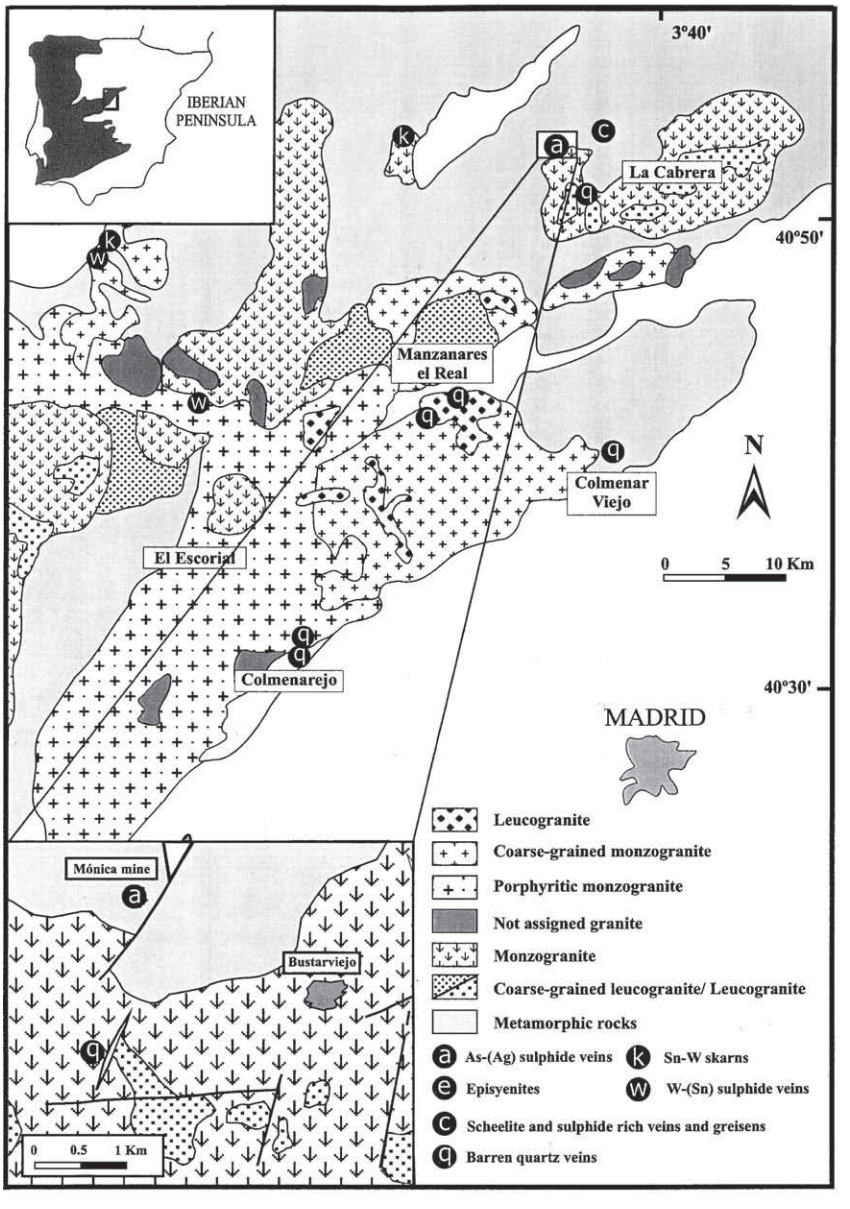

Fig. 1. Simplified map showing the locations of the different Permian mineralisations of the Spanish Central System and sketch map of the studied area. Legend: (1) Leucogranite; (2) Coarse-grained monzogranite; (3) Porphyritic monzogranite; (4) Granite (unassigned); (5) Monzogranite; (6a) Coarse-grained leucogranite; (6b) Leucogranite; (7) Metamorphic rock; (8) As–(Ag) sulphide veins; (9) Sn–W skarns; (10) Episyenites; (11) Scheelite sulphide-rich veins and greisens; (12) W–(Sn) sulphide veins and related greisens; (13) Barren quartz veins (modified from Villaseca et al., 1998).

reactivation of major fractures, encompassing the late extensional collapse of the Variscan orogen and the beginning of the Alpine orogeny (González Casado et al., 1996). Although a large number of mineralised veins accompanied by hydrothermal alteration occur throughout the granitic and metamorphic country rocks, the deposits are of only minor economic importance. W–(Sn) sulphide veins and related greisens (Vindel et al., 1995, 2000), Sn–W skarns (Casquet and Tornos, 1984), episyenites (Caballero, 1993), barren quartz veins (Martín Crespo et al., 1999; 2002) and scheelite sulphide-rich veins and greisens (Tornos et al., 1993) have all been recognised in the SCS (Fig. 1).

The As–(Ag) sulphide vein system of Mónica mine at Bustarviejo (SCS, Madrid province) is a good example of a hydrothermal event probably developed during the Permian times. This uneconomic deposit had not been studied in detail and previous work focused on the textures and mineral associations (Martinez Frías et al., 1984). The presence of a complex paragenetic sequence, and the possibility of tracing different types of fluids, makes this deposit particularly interesting in the context of understanding the regional geological evolution.

Very little was previously known about the fluid chemistry, the conditions of sulphide deposition and age of the mineralisation in the Mónica mine. Thus, the objectives of this work are twofold: (1) to characterise the nature and origin of the mineralising fluids by studying: (i) the relative chronology of the ore minerals from textural and paragenetic relationships, (ii) the $P–T–V–X$ properties of the fluids from fluid inclusion studies, (iii) the origin of the mineralising fluids from the isotope composition of quartz, muscovite and sulphides; and (2) to date the hydrothermal event responsible for the sulphide mineralisation. Finally, by combining the obtained results with the available geological, mineralogical and geochemical data from other contemporaneous dated hydrothermal mineral deposits reported in the area, it will be possible to place the As–(Ag) sulphide veins within the general evolution of the hydrothermal events in the SCS.

2. Geological setting

The Mónica mine is located in the Sierra de Guadarrama, central part of the SCS (Fig. 1). This area is characterised by the presence of granitoids and high- to medium-grade metamorphic rocks. Recurrent tectonic activity along master faults is recorded at different ages and persists to the present (Casquet et al., 1988; Doblas et al., 1994). Metamorphic rocks include abundant pre-Variscan peraluminous orthogneisses of Early Ordovician age (Vialette et al., 1987), pelitic and semipelitic paragneisses, migmatitic banded gneisses and detrital and carbonate rocks of Precambrian–Devonian age. Petrological and geochronological studies indicate the acid igneous pre-metamorphic character of these rocks and their intrusion between the Middle Cambrian and Lower Ordovician. $^{87}Rb/^{86}Sr$ whole-rock data give a minimum emplacement age for the orthogneisses between 500 and 470 Ma (Vialette et al., 1987).

As–Ag-bearing mineralised veins crosscut felsic augen–orthogneisses and some medium-grained leucogneisses. The augen-gneisses exhibit a typical high-temperature assemblage of biotite, sillimanite, metastable andalucite and garnet, together with quartz, K-feldspar and plagioclase. In some mesocratic bands, cordierite can be also present. Typical accessory phases include apatite, zircon and ilmenite. The augen are composed of perthitic K-feldspar with inclusions of biotite, quartz and plagioclase crystals. Interbanded with these are quartz–feldspar-rich types of leucogneiss, with typical tourmaline-rich lenses. Their protolith can be identified as megacrystic granites and leucogranites (Escuder et al., 1998). Metasedimentary rocks and orthogneisses have been affected by high-grade mertamorphism with local to extensive anatexis. The high metamorphic grade has led to the progressive formation of migmatitic structure and stromatic, ptygmatic, schlieren and nebulitic structures are distinguished. Digested xenoliths and some residual augen feldspar can be observed coming from the orthogneisses.

Granitic plutonism postdates the main tectono–metamorphic events. Plutonic magmatism is concentrated from 345 to 284 Ma (Villaseca et al., 1995), following the main peak of the Hercynian orogeny and encompassing the late extensional collapse of the orogen. The granitoids are mostly peraluminous monzogranites and leucogranites, with minor intrusions of more mafic composition. They are geochemically homogeneous showing a restricted range of granite

types. Geochemical and isotope features of SCS granitoids are compatible with felsic lower crustal sources (Villaseca and Herreros, 2000). The La Cabrera granite is located 250 m south of the Mónica mine (Fig. 1), and represents the easternmost granite intrusion in the SCS. Contacts with the country rocks are intrusive and disharmonic with the regional structure and produced a contact aureole. $^{87}Rb/^{86}Sr$ age determinations range from 310 ± 14 to 288 ± 5 Ma (Vialette et al., 1981). The massif is composed of several petrographic varieties, where the main facies comprises medium- to coarse-grained biotite granites and monzogranites. Related to this marginal facies appears a large apical body of medium- to fine-grained, highly evolved leucogranites. The contact between the marginal and the central facies is gradational. Pegmatitic veins and miarolitic cavities filled by postmagmatic hydrothermal Ca-rich minerals are abundant in the most evolved granite (Lozano et al., 1999; González Laguna et al., 2000).

The Mónica mine was developed in an As–(Ag) mineralised stockwork and currently has only minor economic significance. The workings have been described by (Samper, 1977). Silver was first discovered in the 17th century and the most mining activity occurred in the period from 1866 to 1877. The distribution of the metals (Ag and Cu) seems to be very irregular and only in some veins and cavities do bonanza grade accumulations occur. In the year 1870, the mine produced around 350 kg of Ag at a grade of 120 g/t, and 1600 kg of Cu. From 1877 until its closure in 1926, the mine was worked periodically. Since then, only sporadic mining and exploration has taken place in the area. The mineralisation consists of irregular and relatively thin (<10 cm) mineralised tension gashes and cavities following a major N30–35°E strike, which may be considered as type I structures. They are filled with quartz and sulphides and crosscut augen orthogneisses and migmatites. Both wallrock and veinlets are characteristically brecciated as a consequence of successive hydrothermal events. The deposit is located 250 m north of the La Cabrera monzogranite. Local hydrothermal alteration (sericitisation and chloritisation) affecting the wallrock around veinlets is recognised. Sericite is generated by alteration of feldspars and chloritisation is restricted to the alteration of biotite.

3. Analytical methods

Compositional analyses of sulphides (arsenopyrite, pyrite, sphalerite, chalcopyrite, pyrrhotite, stannite, galena, native bismuth and Ag–Bi–Pb sulphosalts) and muscovite were carried out using a JEOL Superprobe JXA-8900 M electron microprobe (Universidad Complutense) with an acceleration voltage of 20 kV for sulphides and 15 kV for muscovite.

Microthermometric studies of fluid inclusions (≈ 180 inclusions from 24 samples) were carried out on doubly polished wafers (≈ 300 μm in thickness) using a Linkam THMSG 600 heating–freezing stage. The stage was calibrated with melting point of solid standards at $T>25$ °C, and natural and synthetic inclusions at $T<0$ °C. The rate of heating was monitored in order to get an accuracy of ± 0.2 °C during freezing, ± 1 °C when heating over the 25–400 °C range, and ± 4 °C over the 400–600 °C range. Salinity of H_2O–NaCl inclusions, reported as equivalent wt.% NaCl, was calculated from microthermometric data using the equations from Bodnar (1993). Molar fractions of CO_2, CH_4 and N_2 in the gas phase were determined in individual fluid inclusions by micro-Raman analysis with a DILOR X–Y multichannel modular Raman spectrometer at CREGU, Nancy (France). Bulk composition and molar volume were computed from P–V–T–X properties of individual inclusions in the C–O–H–(N–S) system (Thiery et al., 1994; Bakker et al., 1996) using an estimation of the NaCl content but neglecting the effect of sulphate content. The P–T properties of aquo-carbonic inclusions were modelled for the system H_2O–NaCl–CO_2–CH_4 using the V–X data and the equation of state of Bakker (1999) and data from Zhang and Frantz (1987) for the H_2O–NaCl system.

Irradiation and stepwise heating of micas was done according to the method of Kamber et al. (1995). Ten milligrams of mica were handpicked to achieve visual purity of ~ 100%. The selected samples were irradiated in the Risø reactor (Denmark), and step-heated in a double-vacuum resistance oven connected to a MAP 215-50B mass spectrometer. The analyses were carried out at the Mineralogisches Institut, Bern (Switzerland).

Sulphur isotope compositions of sulphides (arsenopyrite, sphalerite, pyrite and chalcopyrite) were analysed at the Serveis Científico-Tècnics, University

of Barcelona, using an on-line elemental analyser (EA)-continuous flow-isotope ratio mass spectrometer (IRMS). The isotope ratios were calculated using the NBS127, IAEAS1 and IAEAS3 standards and are reported as ‰ deviation relative to the Canyon Diablo troilite (CDT) standard. Precision was better than ± 0.1‰.

$\delta^{18}O$ and δD analyses were carried out at the Activation Laboratories (Ancaster, Ontario, Canada). Mica samples for δD analyses were outgassed in a vacuum at 120 °C for 4 h to remove surface-adsorbed water. The sample was then inductively heated at 1400 °C for up to 20 min and the gases were collected in a trap held at − 196 °C. The water was reacted with uranium at 900 °C to produce H_2 and collected on charcoal at − 196 °C. Isotopic analyses, made by conventional isotope ratio mass spectrometry, are reported in the familiar notation in per mil relative to the V-SMOW standard. $\delta^{18}O$ of silicate samples were reacted with BrF_5 at ≈ 650 °C in nickel furnaces following the procedures described by Clayton and Mayeda (1963). Evolved O_2 was subsequently converted to CO_2 gas using a hot C rod. Isotopic analyses were performed on a Finnigan MAT Delta, dual inlet, isotope ratio mass spectrometer. The data are reported in the standard delta notation as per mil deviations from V-SMOW.

4. Vein mineralogy

The mineral association found in the studied samples is generally in agreement with data from previous studies (Vindel, 1980; Martinez Frías et al.,

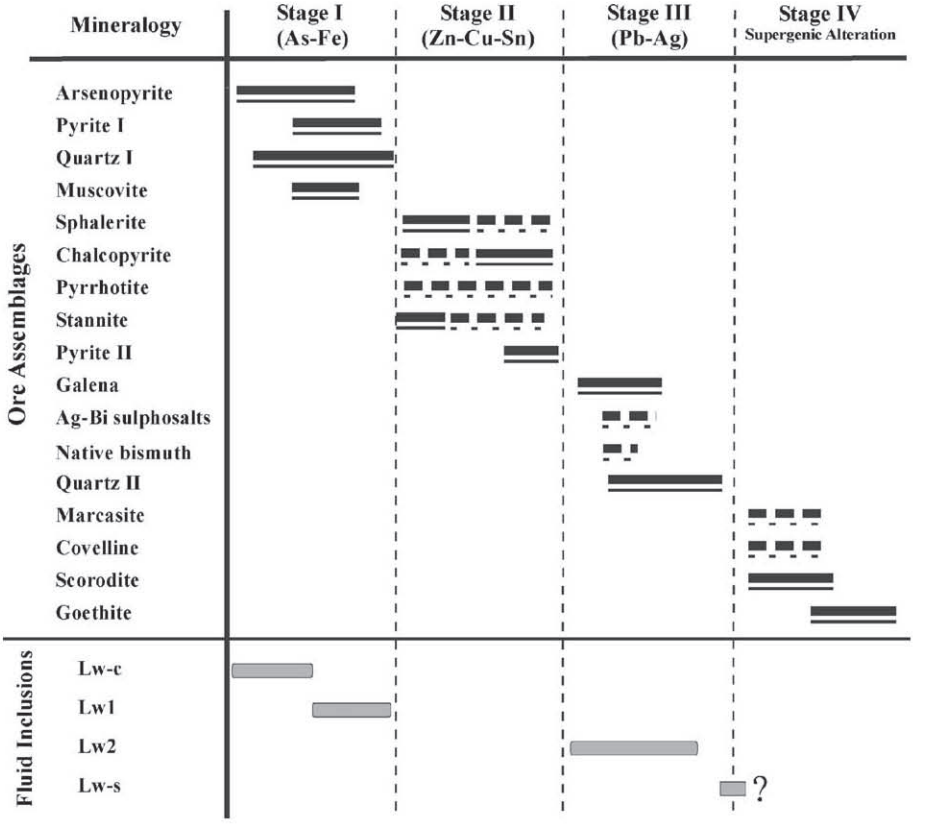

Fig. 2. Paragenetic sequence and distribution of fluid inclusion types in the main ore and alteration assemblages at Mónica mine (line discontinuities represent minor abundances of the minerals formed). Lw-c: aqueous–carbonic fluid inclusions; Lw1 and Lw2: undersaturated aqueous fluid inclusions; Lw-s: hypersaline aqueous fluid inclusions.

1984), although some mineral phases had been incorrectly described, and others went unrecognised prior to this study. The veins are characterised by multistage ore deposition, belonging to four mineralising stages. The paragenetic sequence is given in Fig. 2 and the composition of ore minerals reported in Table 1.

4.1. Ore stage I (As–Fe)

Ore stage I is characterised by the occurrence of arsenopyrite, pyrite, muscovite and quartz (Fig. 3a). Arsenopyrite formed early in the vein sequence, overlapping temporally with pyrite, and occurs as subeuhedral crystal aggregates or needle-like prisms. Pyrite forms euhedral grains, such as cubes or truncated cubes. The As content of arsenopyrite shows a limited compositional range (44.3 ± 2.30 wt.%). Similarly, the variation in Fe content is also very small: 35.5 ± 0.45 wt.%. The total concentration of Ni and Co does not exceed 0.1 wt.%.

Muscovite, which had not been described in the previous studies, was deposited early in the paragenetic sequence and occurs as inclusions and also around the outer margins of coetaneous arsenopyrite, pyrite and quartz; radial and rosette-like aggregates are commonly observed. Microprobe analyses indicate that the mica is muscovite with insignificant illite substitution (Table 2). Quartz I (QI) is intergrown with arsenopyrite, pyrite and muscovite. These early milky quartz crystals show heterogranular, sub-euhedral and rounded shapes in cross-section, with corroded margins where appear together with micas. Brittle deformation of the ore is recognizable from the cataclastic textures of arsenopyrite (Fig. 3b), pyrite and quartz, and development of microfractures healed by subsequent ore minerals.

4.2. Ore stage II (Zn–Cu–Sn)

The second stage is characterised by the cogenetic crystallisation of sphalerite, chalcopyrite, stannite and pyrite, and the presence of pyrrhotite as an exsolved phase in sphalerite. Several textural types have been observed in the sulphide intergrowths. Sphalerite mainly fills microfractures in minerals of ore stage I, and contains blebs and lamellae of chalcopyrite, stannite and pyrrhotite, the most char-

Table 1
Electron microprobe analysis (means, wt. %) of the main ore minerals from Mónica mine

Mineral	Asp	Py	Sl	Cp	Po	St	Gn	Native Bi
Number of analyses	18	20	15	14	5	15	15	4
	Stage I (wt.%)		Stage II (wt.%)				Stage III (wt.%)	
As	44.26	0.04	<mdl	<mdl	<mdl	<mdl	<mdl	<mdl
Pb	0.09	0.11	0.08	0.20	0.16	0.08	83.08	<mdl
Ag	<mdl	<mdl	<mdl	0.03	<mdl	<mdl	1.00	<mdl
S	20.67	52.54	33.18	35.15	39.42	29.99	13.72	0.11
Bi	0.09	0.21	0.10	0.11	0.12	0.09	2.65	99.84
Fe	35.49	46.65	11.20	29.80	59.52	13.09	0.09	0.11
Cd	<mdl	<mdl	0.56	<mdl	<mdl	<mdl	0.21	<mdl
Zn	<mdl	<mdl	51.97	0.11	<mdl	1.43	<mdl	<mdl
Mn	<mdl	<mdl	0.98	<mdl	<mdl	<mdl	<mdl	<mdl
Sb	<mdl	0.03	0.04	<mdl	0.03	<mdl	<mdl	0.10
Au	<mdl	<mdl	0.37	<mdl	<mdl	<mdl	<mdl	<mdl
Co	0.10	0.07	<mdl	0.03	0.06	<mdl	<mdl	<mdl
Sn	<mdl	<mdl	0.09	0.28	<mdl	26.56	0.03	<mdl
Cu	<mdl	<mdl	0.85	33.59	<mdl	28.32	<mdl	<mdl
Total	100.70	99.65	99.42	99.30	99.31	99.56	100.78	100.16

Asp: arsenopyrite, Py: pyrite, Sl: sphalerite, Cp: chalcopyrite, Po: pyrrhotite, St: stannite, Gn: galena.
Minimum detection limits (ppm)—As: 200; Pb: 200; Ag: 160; S: 140; Bi: 350; Fe: 130; Cd: 100; Zn: 75; Mn: 190; Sb: 140; Au: 200; Co: 100; Sn: 170; Cu: 170.

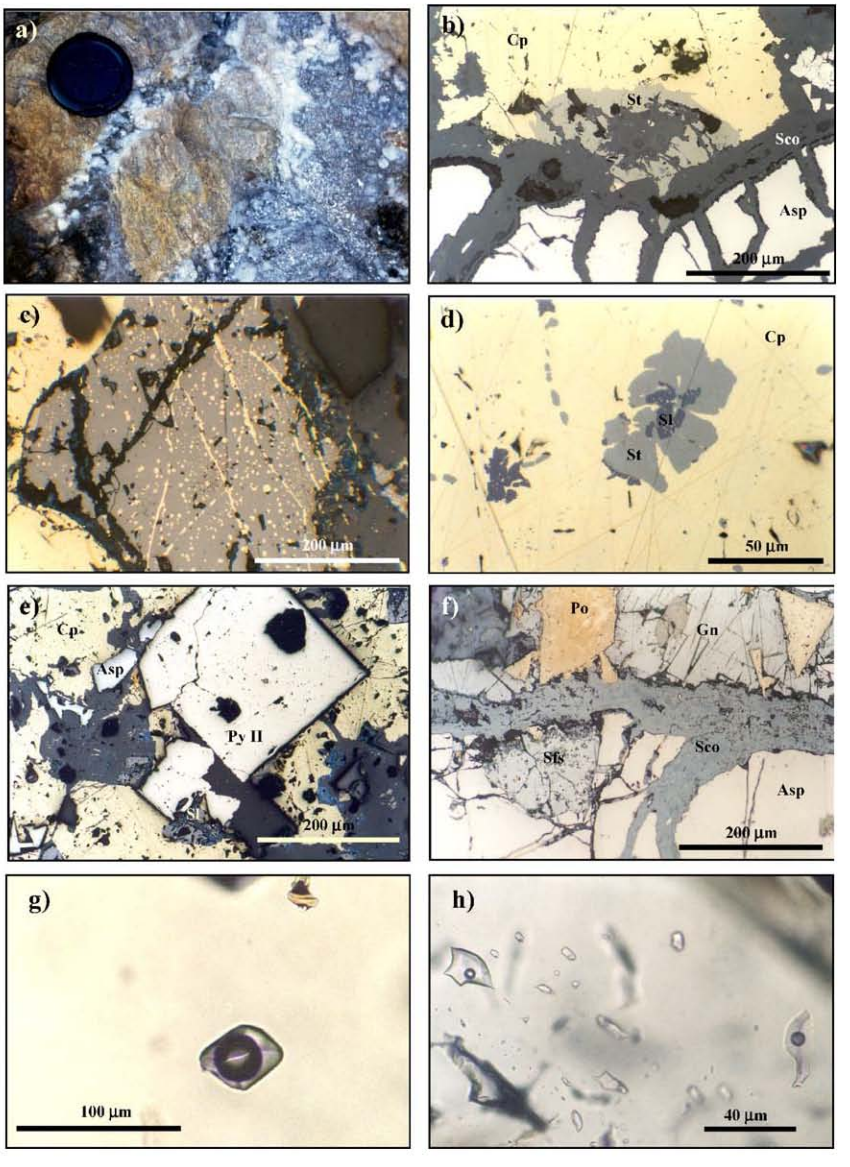

Fig. 3. (a) Arsenopyrite, pyrite and quartz filling veins and cavities in brecciated orthogneisses; (b) arsenopyrite (Asp) replaced by scorodite (Sco) along microfractures. Chalcopyrite (Cp) associated with stannite (St) can be observed; (c) "chalcopyrite disease" texture, showing blebs and lamellae of chalcopyrite linearly distributed along several directions; d) coarse grains of chalcopyrite (Cp) including star-like exsolutions of stannite (St) and sphalerite (Sl); (e) euhedral crystal of pyrite II (Py II) in association with chalcopyrite (Cp). Some corroded crystals of stage I arsenopyrite (Asp) can be observed; (f) arsenopyrite (Asp) replaced by scorodite (Sco). Galena (Gn) and Ag–Bi–Pb sulphosalts (Sfs) filling cavities between pyrrhotite (Po) crystals; (g) isolated primary Lw-c fluid inclusion hosted in quartz QI showing around 50% vapour phase; (h) irregular secondary Lw2 fluid inclusions in quartz QI showing around 15% vapour phase.

acteristic textures of the Mónica ores (Fig. 3c). The chalcopyrite blebs and lamellae make up more than 5% of the sphalerite by volume. The texture had formerly been interpreted as an exsolution processes (Amorós et al., 1984, Martinez Frías et al., 1984). Sphalerite co-precipitated with chalcopyrite is Fe-poor (<5 mol% FeS), hosting triangular or irregularly bleb-like inclusions of chalcopyrite (cf. Nagase

Table 2
Representative electron probe microanalyses and calculated formulae of stage I muscovite

Sample	B-13 (A8)	B-13 (A22)	B-40 (A10)	B-40 (A130)	B-312 (A24)	B-312 (A134)	B-315 (A35)	B-315 (A152)
Oxide (wt.%)								
SiO_2	45.63	45.42	46.01	46.69	46.36	46.55	48.23	47.13
TiO_2	0.87	0.35	0.41	0.49	0.27	0.28	<mdl	0.11
Al_2O_3	36.50	36.88	35.76	35.35	33.96	33.46	33.53	34.44
FeO	0.71	0.73	0.66	0.95	2.16	1.32	0.59	0.63
MnO	0.04	<mdl	<mdl	<mdl	0.03	<mdl	<mdl	0.04
MgO	0.54	0.62	0.53	0.95	1.46	1.86	1.49	1.30
CaO	<mdl	<mdl	0.03	<mdl	0.10	0.04	<mdl	<mdl
Na_2O	0.52	0.52	0.65	0.55	0.38	0.35	0.26	0.42
K_2O	10.30	10.28	10.26	10.70	10.11	10.58	10.65	10.55
F	0.12	0.19	0.32	0.07	0.26	0.28	0.24	0.16
Total	95.23	94.99	94.63	95.75	95.09	94.72	94.99	94.78
Formulae calculated on the basis of 24 (O, OH, F, Cl)								
Si	6.060	6.049	6.154	6.179	6.214	6.256	6.411	6.285
Al^{IV}	1.940	1.951	1.846	1.821	1.786	1.744	1.589	1.715
Σ	8.00	8.00	8.00	8.00	8.00	8.00	8.00	8.00
Al^{VI}	3.769	3.833	3.787	3.688	3.575	3.552	3.659	3.694
Ti	0.087	0.035	0.041	0.049	0.028	0.028	0.000	0.011
Fe	0.078	0.081	0.073	0.105	0.242	0.148	0.065	0.071
Mg	0.107	0.123	0.105	0.187	0.291	0.372	0.296	0.258
Σ	3.769	3.833	3.787	3.688	3.576	3.553	3.659	3.694
Na	0.135	0.135	0.168	0.142	0.100	0.090	0.066	0.109
K	1.745	1.746	1.751	1.807	1.729	1.814	1.806	1.794
F	0.101	0.163	0.267	0.061	0.224	0.234	0.203	0.136
OH (by difference)	3.950	3.918	3.866	3.967	3.887	3.881	3.897	3.931

Minimum detection limit (ppm)—Si: 420; Ti: 220; Al: 125; Fe: 255; Mn: 210; Mg: 120; Ca: 130; Na: 125; K: 115; F: 725.

and Kojima, 1997). Chalcopyrite disease, as seen in samples from Mónica mine, is more likely the result of a replacement process, as suggested by the mean Fe content of sphalerite (22.5 mol% FeS) and the development of lamellar and regular bodies of chalcopyrite (Table 1).

Chalcopyrite also occurs as coarse crystals including minerals from ore stage I. The mineral is intergrown with sphalerite and stannite, and fills microfractures and voids between brecciated arsenopyrite, pyrite and quartz crystals. This type of chalcopyrite contains star-like exsolutions of stannite and sphalerite (Fig. 3d). Stannite is much less abundant than sphalerite and chalcopyrite and occurs as a discrete phase accompanying these ore minerals, and as inclusions in sphalerite and chalcopyrite. Blebs and rods of exsolved pyrrhotite are common in sphalerite and stannite. Ore stage II is characterised by the presence of sphalerite and a noticeable Zn content of cogenetic minerals (chalcopyrite and stannite; Table 1). Finally, euhedral grains of pyrite (pyrite II) are found in association with chalcopyrite (Fig. 3e), sphalerite and filling microfractures within arsenopyrite. Microprobe analysis has not revealed any significant differences in chemical composition between pyrites I and II.

4.3. Ore stage III (Pb–Ag–Bi)

The third stage of mineralisation is characterised by the presence of galena, Ag–Bi–Pb sulphosalts, native bismuth and quartz (QII). Irregular shaped grains of galena fill interstices between minerals, similar to arsenopyrite, pyrite and sphalerite deposited in the previous ore stages (Fig. 3f). Lath-like Ag–Bi–Pb-sulphosalt-galena intergrowths are a characteristic

Table 3
Representative electron microprobe analyses and mineral formulae of Ag–Bi sulphosalts

Sample (wt.%)	B-311 (1)	B-312 (2)	B-25 (3)	B-27 (4)	B-28 (5)	B-312b (6)	B-313 (7)	B-28b (8)
Fe	<mdl	0.04	0.03	<mdl	<mdl	0.03	0.03	0.04
Ag	9.81	10.15	16.10	9.59	9.64	14.26	8.83	15.37
Pb	28.01	29.63	44.01	27.75	30.80	33.00	21.10	30.53
Bi	45.75	43.40	23.19	46.60	43.70	35.62	53.65	38.00
Sb	<mdl	<mdl	0.08	0.07	0.06	<mdl	<mdl	0.04
Sn	<mdl	<mdl	0.44	<mdl	<mdl	<mdl	<mdl	<mdl
S	16.14	16.31	16.10	16.35	15.98	16.02	16.26	16.05
Total	99.71	99.49	99.92	100.36	100.18	98.90	99.84	99.99

Formulae:
(1) $Ag_{1.09}Pb_{1.69}Bi_{2.63}S_6$;
(2) $Fe_{0.01}Ag_{1.13}Pb_{1.79}Bi_{2.49}S_6$;
(3) $Fe_{0.01}Ag_{1.79}Pb_{2.55}(Bi_{1.33}Sb_{0.01}Sn_{0.04})S_6$;
(4) $Ag_{1.07}Pb_{1.61}(Bi_{2.68}Sb_{0.01})S_6$;
(5) $Ag_{1.07}Pb_{1.78}(Bi_{2.51}Sb_{0.01})S_6$;
(6) $Fe_{0.01}Ag_{1.59}Pb_{1.91}Bi_{2.05}S_6$;
(7) $Fe_{0.01}Ag_{0.98}Pb_{1.22}Bi_{3.08}S_6$;
(8) $Fe_{0.01}Ag_{1.71}Pb_{1.77}Bi_{2.18}S_6$.
Minimum detection limit (ppm)—Fe: 180; Ag: 160; Pb: 150; Bi: 380: Sb: 175: Sn: 180; S: 125.

feature of this mineralisation stage. Sulphosalts from Mónica mine were firstly described by Ramdohr (1969) as matildite, $AgBiS_2$, and interpreted as an exsolved phase parallel to the (111) planes of host galena. However, our electron microprobe analysis excludes the presence of matildite. Compositional variation among lamellar Ag–Bi–Pb-bearing phases ($Ag_{0.98-1.79}Pb_{1.22-2.55}Bi_{1.33-3.08}S_6$) corresponds mainly to the compositional range of lillianite homologues or "schirmerite" (Foord and Shawe, 1989), possibly partly reflecting 'bulk' analyses of extremely fine-grained intergrowths (Table 3). Minor amounts of native bismuth are widespread in association with Ag–Bi sulphosalts and galena.

Ore stage III is characterised by the presence of quartz (QII) that appears as crystal aggregates overlapping the deposition of galena and, to some extent, Ag–Bi–Pb minerals. In some instances, quartz (QII) occurs as euhedral crystals filling vug cavities and ranging from a few millimetres up to 5 cm in size.

Table 4
Fluid inclusion microthermometric and Raman microprobe data of the different fluid inclusions types represented in As–(Ag) veins

	Aqueous–carbonic fluid	Aqueous fluids		
Inclusion type	Lw-c	Lw1	Lw2	Lw-s
Components	H_2O–NaCl–CO_2–CH_4	H_2O–NaCl	H_2O–NaCl	H_2O–NaCl
Phases at room temperature	Two phases	Two phases	Two phases	Three phases
Vapour (%)	40–50	30–50	15–45	5–10
T_{CL} (°C) (25)	5.7–8.5, mode: 8.5	–	–	–
T_{MICE} (°C) (175)	−3.7 to −2.2, mode: −3.3	−1.9 to −0.5, mode: −1	−1 to 0, mode: −0.2	−45 to −40, mode: –
T_S (°C) (3)	–	–	–	100–115, mode: –
T_H (°C) (143)	335–365, mode: 360	315–360, mode: 350	160–255, mode: 200	60–70, mode: –
Salinity (eq. wt.% NaCl)	3–8, mode: 3	0.8–3.1 mode: 1.7	0–1.5, mode: 0.3	30–35, mode: –
Density (g/cm^3)	0.5–0.65, mode: 0.55	0.6–0.65, mode: 0.63	0.8–0.9, mode: 0.85	0.25–0.28, mode: –
CO_2 (mol%)	68–81.6	–	–	–
CH_4 (mol%)	18.4–26	–	–	–
N_2 (mol%)	0–7.9	–	–	–

T_{CL}: clathrate melting; T_{MICE}: last ice melting; T_S: last solid melting; T_H: homogenisation to liquid; (175) = number of measurements.
Considering that Lw-s inclusions are quite scarce, modal values cannot be considered as representative.

4.4. Stage IV: supergene alteration

Early mineral assemblages are locally replaced by supergene marcasite, covellite, scorodite and goethite (Fig. 2). This low-temperature alteration assemblage is found in complex sets of micro-cracks that crosscut the earlier minerals.

5. Fluid inclusion study

On the basis of textural relationships, microthermometry and Raman microprobe data, four types of fluid inclusions have been distinguished. Fluid inclusion types are described according to the criteria of Boiron et al. (1992), based on the nature of the dominant chemical phases and the type of phase change. Microthermometric and Raman microprobe data on selected fluid inclusions are summarised in Table 4.

Two major types of fluids have been recognised from petrographic observations and microthermometric measurements: early aqueous–carbonic fluids exclusively related to stage I minerals (Lw-c inclusions), and aqueous fluids related to minerals from stage I (Lw1 inclusions) and stage III (Lw2 and Lw-s inclusions).

Lw-c: isolated primary inclusions (liquid + vapour) distributed along growth planes at the margin of QI idiomorphic crystals, in contact with arsenopyrite (Fig. 3g). **Lw1**: randomly distributed inclusions (liquid + vapour) mostly as negative crystals and spatially associated to Lw-c inclusions. **Lw2**: sub-idiomorphic fluid inclusions (liquid + vapour), trapped later than Lw1, secondary in QI and pseudosecondary in QII. Both types are ubiquitous in all samples, but Lw1 are dominant in QI and Lw2 in QII (Fig. 3h). **Lw-s**: they exhibit three phases (liquid + vapour + solid) at room temperature. These are scarce and irregularly shaped, occur along secondary healed fracture planes in QI and QII, and represent the last hydrothermal event recognised in the As–(Ag) veins (Fig. 2).

5.1. Aqueous–carbonic fluids

The Lw-c type contains a H_2O–NaCl–CO_2–CH_4 fluid characterised by a melting ice temperature (T_{MICE}) range between −3.7 and −2.2 °C, and a volatile phase dominated by CO_2 (68–81.6 mol%) with variable CH_4 (18.4–26 mol%) and N_2 (n.d. to 7.9 mol%) contents. Salinity calculated from melting temperature of clathrate (T_{CL} from 5.7 to 8.5 °C with a mode at 8.5 °C), and from volatile composition determined by Raman analysis, is in the range 0.4–8 wt.% NaCl eq. Total homogenisation to the liquid

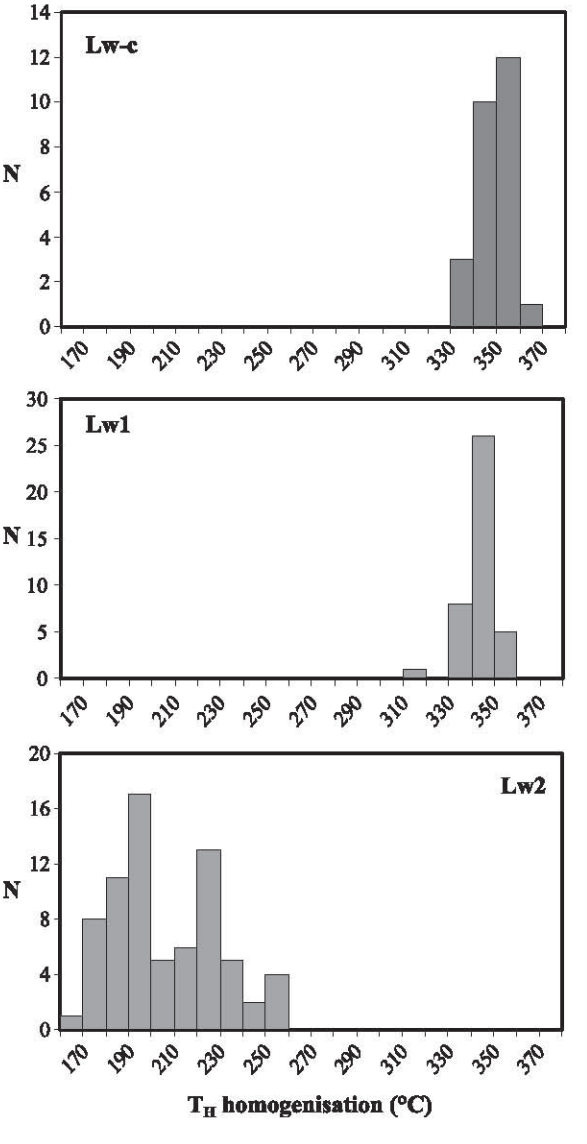

Fig. 4. Homogenisation temperature histograms for Lw-c, Lw1 and Lw2 fluid inclusion types.

phase (T_H) is between 335 and 365 °C, with 360 °C as the modal value (Table 4).

5.2. Aqueous fluids

Lw1 two-phase inclusions are fluids belonging to the H_2O–NaCl system. They have low salinity, displaying a T_{MICE} in the range of −1.9 to −0.5 °C (0.8 to −3.1 wt.% NaCl eq.; mode 1.7 wt.%). No eutectic temperature could be determined. T_H (Fig. 4) occurs to the liquid phase in the range of 315–360 °C (mode 350 °C).

Lw2 are two-phase inclusions containing a H_2O–NaCl fluid. They display lower T_{MICE} (−1 to 0 °C, mode −0.2 °C), corresponding to salinities of 0–1.5 wt.% NaCl eq. (mode 0.3 wt.%), and T_H between 16 and −255 °C (mode 200 °C), both lower than Lw1 inclusions (Fig. 4). No C–H–O–(N–S) species have been detected by Raman microprobe in the non-aqueous phase of Lw1 and Lw2 inclusions.

Lw-s hypersaline inclusions exhibit three phases at room temperature, and are defined by a low-temperature (T_H: 60–70 °C) H_2O–NaCl fluid. Salt content has been estimated from halite melting (100–115 °C) corresponding to salinities of 30–35 wt.% NaCl eq.

6. Stable isotopes

In order to gain insight into the origin of the fluids involved in vein formation, quartz from stages I (QI) and III (QII) and muscovite (stage I) were analysed for their stable isotope composition. Results are presented in Table 5.

The $\delta^{18}O$ of muscovite ranges from 6.9‰ to 8.5‰, and δD ranges from −52‰ to −38‰. Stage I quartz

Table 5
Stable isotope values of silicates and sulphides from Mónica mine

Mineral	Stage	Sample	$\delta^{18}O$ (‰)	δD (‰)	$\delta^{34}S$ (‰)	$\delta^{18}Ow$ (‰)	δDw (‰)
Quartz I	I	B-33	+10.9			+5.5	
Quartz I	I	B-31	+13.1			+7.7	
Quartz I	I	B-5	+12.1			+6.7	
Quartz I	I	B-34	+15.2			+5.3	
Quartz II	III	B-1	+11.4			−2.3 to −1.5	
Quartz II	III	B-4	+14.2			+0.4 to +4.3	
Quartz II	III	B-7	+13.0			−0.7 to +3.0	
Quartz II	III	B-9	+14.1			+0.3 to +4.2	
Muscovite	I	Bu-19	+6.9	−47		+6.4	−11.0
Muscovite	I	Bu-131	+8.3	−38		+7.8	−2.0
Muscovite	I	Bu-133	+8.0	−52		+7.5	−16.0
Muscovite	I	Bu-233	+8.5	−43		+8.0	−7.0
Arsenopyrite	I	B-24			+2.8		
Arsenopyrite	I	B-28			+3.6		
Arsenopyrite	I	B-31			+2.0		
Arsenopyrite	I	B-33			+2.6		
Arsenopyrite	I	B-91			+2.5		
Arsenopyrite	I	B-311			+2.4		
Pyrite	II	B-28			+2.2		
Pyrite	II	B-92			+2.1		
Pyrite	II	B-292			+2.3		
Chalcopyrite	II	B-27			+2.0		
Chalcopyrite	II	B-93			+1.5		
Sphalerite	II	B-28			+1.9		
Sphalerite	II	B-94			+2.9		
Sphalerite	II	B-291			+2.2		

$\delta^{18}Ow$ and δDw correspond to the isotopic composition of water in equilibrium with quartz and muscovite.
Calculations were performed at 360 °C for stage I quartz (QI) and muscovite, and between 170 and 230 °C for stage III quartz (QII) (see text for explanation). The equations of Zheng (1993) and Suzuoki and Epstein (1976) were used for oxygen–water and deuterium–water fractionations, respectively.

(QI) coexisting with muscovite has $\delta^{18}O$ values from 10.9–15.2‰ and $\delta^{18}O$ of quartz (QII) from stage III has values between 11.4‰ and 14.2‰. Assuming a minimum T of formation for QI of 360 °C (fluid inclusion data) and using the equation of Zheng (1993) for quartz–water O-isotope fractionation, the calculated minimum $\delta^{18}O$ value of water in equilibrium with quartz is between +5.5‰ and +9.8‰.

The $\delta^{18}O$ of water in equilibrium with muscovite (calculated from Zheng, 1993), at 360 °C, shows a more limited minimum range (+6.5–8.0‰), whereas water δD varies from −2‰ to −16‰ (calculated from Suzuoki and Epstein, 1976). Taking a *T* range of between 170 and 230 °C during QII formation, the calculated isotope composition of water in equilibrium with quartz ranges from −2.3‰ to +4.3‰. Coexisting quartz–muscovite pairs show fractionation values between 4‰ and 6.7‰ which correspond to equilibrium temperatures (using the equation of Zheng, 1993) between 190 and 380 °C for the stage I mineral assemblage.

The sulphur isotope composition of stage I arsenopyrite and pyrite and stage II chalcopyrite and sphalerite is quite homogeneous with $\delta^{34}S$ values between +1.5‰ and +3.6‰. The highest value corresponds to an arsenopyrite from stage I, and the lowest to a chalcopyrite from stage II. At the temperatures assumed for sulphide precipitation (>360 °C for stage I, 250 °C for stage II), the $\delta^{34}S$ of sulphides would be almost equal to $\delta^{34}H_2S$ of the fluid.

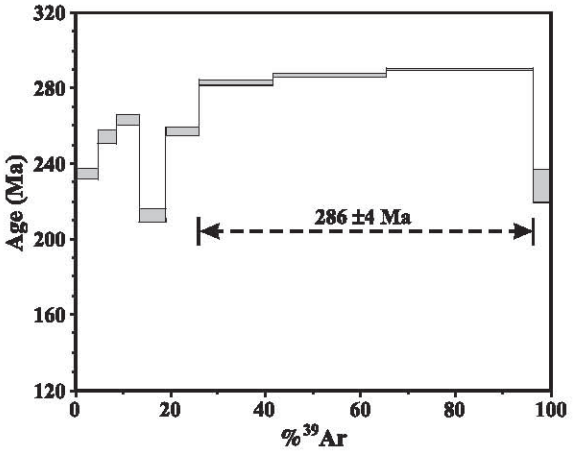

Fig. 5. Age spectrum of stage I hydrothermal muscovite. The spectrum obtained has a staircase shape and the "plateau" is depicted by three of the four late steps.

7. Geochronology

Hydrothermal muscovites coeval with sulphides of the early As–Fe stage have been dated, using the Ar^{39}/Ar^{40} method, to provide constraints on the age of stage I mineralising event. The spectrum obtained has a staircase shape (Fig. 5). A "plateau" age of 286 ± 4 Ma is suggested by three of the four late steps between 26% and 95% fractional ^{39}Ar release. The steps with the lowest age could be explained by diffusion processes and some post-crystallisation heating, mainly at the border of the mineral grains, due to the effects of the later hydrothermal events. Villa (1998) has shown that fluid–mineral interaction is more relevant for isotopic exchange compared to the thermal history of a mineral.

Several Permian hydrothermal events have been recognised in the SCS (Caballero et al., 1992), between 295 ± 10 Ma (W–Sn sulphide veins) and 267 ± 7 Ma (scheelite–sulphide-rich veins). The muscovite age determined in this study (286 ± 4 Ma.), corresponding to the earliest hydrothermal event at Mónica mine, is synchronous with the late emplacement and cooling phases of the La Cabrera massif (Vialette et al., 1981). In fact, this hydrothermal event ranging between 300 and 285 Ma has been interpreted as the result of the emplacement of small granitic intrusions across the region (Tornos et al., 2000).

8. Discussion

8.1. Fluid evolution and PT estimation

The *P–T–X* evolution of the fluids can be reconstructed from the T_H–salinity plot (Fig. 6). The H_2O–NaCl–CO_2–CH_4 (Lw-c) fluid found in stage I quartz, displays a wide salinity range (3–8 wt.% NaCl eq.) over a similar T_H range (335–365 °C). The H_2O–NaCl fluid (Lw1) found in stage I quartz displays a similar T_H range than the aqueous–carbonic fluid but has a lower salinity. The continuous trend in salinity could be interpreted as the result of isothermal mixing between two fluids of contrasting salinity. Stage III is

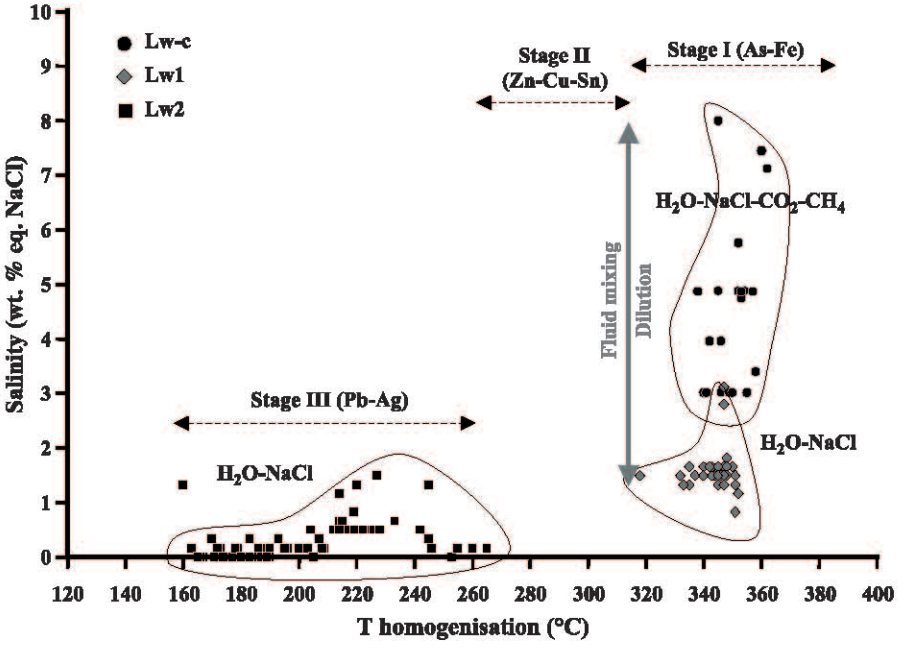

Fig. 6. T_H-vs.-salinity plot for $H_2O-NaCl-CO_2-CH_4$ (Lw-c fluid inclusions) and $H_2O-NaCl$ fluids (Lw1 and Lw2 fluid inclusions).

defined by the presence of a fluid belonging to the $H_2O-NaCl$ system and is characterised by lower T_H (160–260 °C) and similar salinity (< 1.5 wt.% eq. NaCl) than high-temperature $H_2O-NaCl$ inclusions. Low-temperature $H_2O-NaCl$ fluid inclusion population display a wide T_H range reflecting a progressive cooling from 260 to 160 °C, and a slightly decrease of salinity. The whole evolution is contemporaneous with a global density increase from the earliest aqueous–carbonic fluid (density ranging from 0.6 to 0.65 g/cm^3) to the densest low-temperature aqueous fluid (density ranging from 0.8 to 0.9 g/cm^3).

Fig. 7 shows a schematic reconstruction of $P-T$ conditions during the entrapment of the fluids. Early mineralising fluids (stage I) are represented by aqueous–carbonic and aqueous fluid inclusions. The minimum trapping temperatures (T_H) defined by the modal isochores of both fluids vary between 335 and 365 °C. This ore stage is characterised by the coexistence of muscovite and quartz, but if equilibrium is assumed, the estimated isotopic temperature from the oxygen isotope composition of both minerals range from 190 to 380 °C. The similar temperature obtained from fluid inclusion data and from the muscovite–quartz geothermometer suggests that isotopic equilibrium was not attained, since this coincidence would point to vein formation close to the surface. At these temperatures, boiling should have occurred and this has not been observed. Given that the muscovite–quartz pair cannot be used as a geothermometer, the minimum $P-T$ conditions of the As–Fe stage can be only established from fluid inclusion data (350 °C and 0.3 kbar).

Although no minerals suitable for fluid inclusion studies were found in stage II minerals, a temperature approach could be obtained from mineral assemblages using the stannite–sphalerite geothermometer (Nakamura and Shima, 1982). In the Cu–Fe–Zn–Sn–S system, partitioning of Zn and Fe between coexisting stannite and sphalerite may be used to constrain the equilibrium temperature between the two phases. Using the Nakamura and Shima equation, a temperature range of 250–300 °C was obtained, which appears to be in good agreement with that deduced from the whole $P-T$ evolution of the system. Although the mineral assemblage provides no constraints on the pressure conditions, a hydrostatic regime is assumed (Fig. 7).

The latest stage of ore deposition (stage III) is characterised by the circulation of $H_2O-NaCl$ fluids,

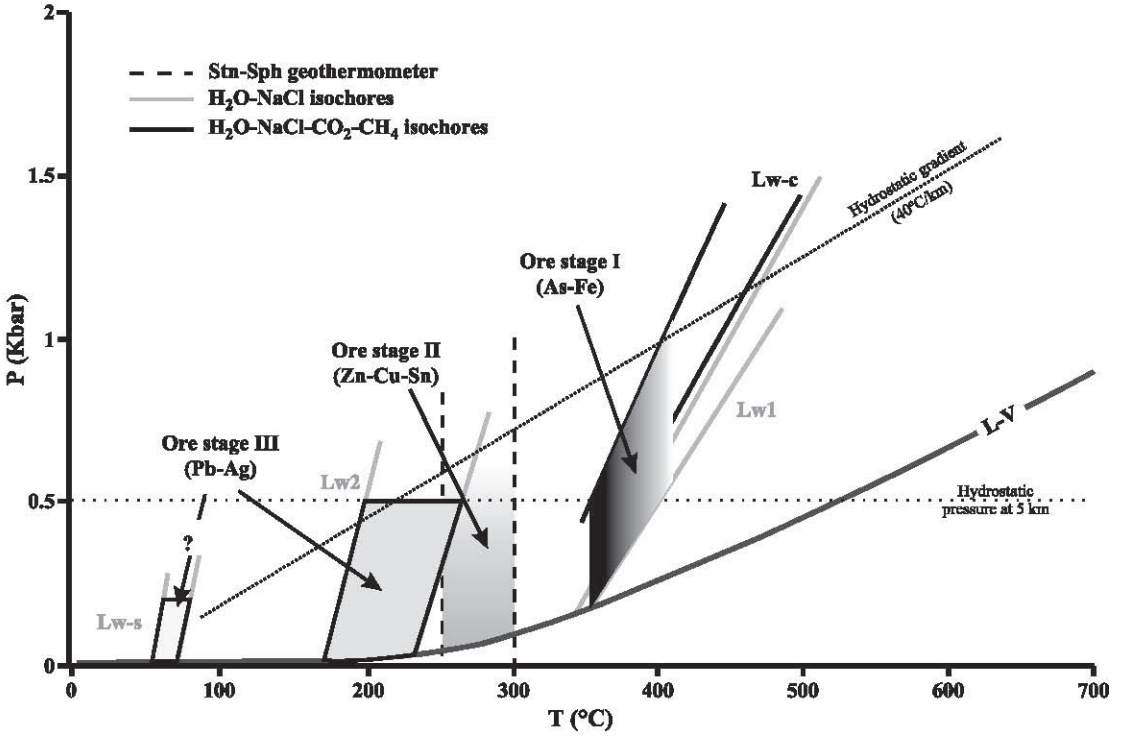

Fig. 7. Reconstruction of the pressure–temperature conditions at Mónica mine during vein formation from modal isochores, mineral geothermometry data and probable trapping conditions of the different group of fluid inclusions. The dashed line represents a thermal gradient of 40 °C/km for a hydrostatic regime.

displaying lower trapping temperatures (defined by modal isochores) between 170 and 230 °C. The absence of any evidence for boiling in Lw2 and Lw-s inclusions, the presence of vuggy textures and the brittle nature of the host gneiss have been taken as indicators of an almost hydrostatic pressure regime during the circulation of this fluid. H_2O–NaCl fluids of meteoric origin have been recognised in all mineralisation types of the SCS (Vindel et al., 2000). Maximum fluid pressures can be constrained by the maximum depth of burial of the enclosing rocks. Late Hercynian granites in the SCS were emplaced at depths of between 5 and 8 km, under a lithostatic pressure of ≈ 2 kbar (Villaseca et al., 1998). According to an almost hydrostatic pressure regime for ore stage III, a minimum depth of 5 km indicates a P_{fluid} of 0.5 kbar.

The dominant mechanism of As–Fe ore deposition during stage I could be interpreted as a mixing process between aqueous–carbonic (Lw-c) and aqueous (Lw1) fluids (Fig. 6) at temperatures and pressures around 400 °C and <1 kbar, respectively (Fig. 7). In this type of environment, As–(Fe) transport and sulphide deposition are usually related to the presence of aqueous–carbonic fluids equilibrated with metamorphic rocks (Noronha et al., 1995), and related to dilution and cooling (mixing) with other fluids. As mentioned above, at a minimum temperature of 360 °C, the $\delta^{18}O$ of water in equilibrium with stage I quartz is between +5.3‰ and +7.7‰, and the δD of water in equilibrium with coexisting muscovite is from −2.0‰ to −16.0‰. In a $\delta^{18}O/\delta D$ diagram, these values plot within or close to the metamorphic water field (Sheppard, 1986) (Fig. 8). This is taken to imply that isotopic composition of stage I mineralisation could be related to waters isotopically equilibrated with the basement (either metamorphic or igneous rocks). This origin is supported by the sulphur isotope composition of sulphides. The $\delta^{34}S$ range (+1.5–3.6‰) points to an isotopically homogeneous source,

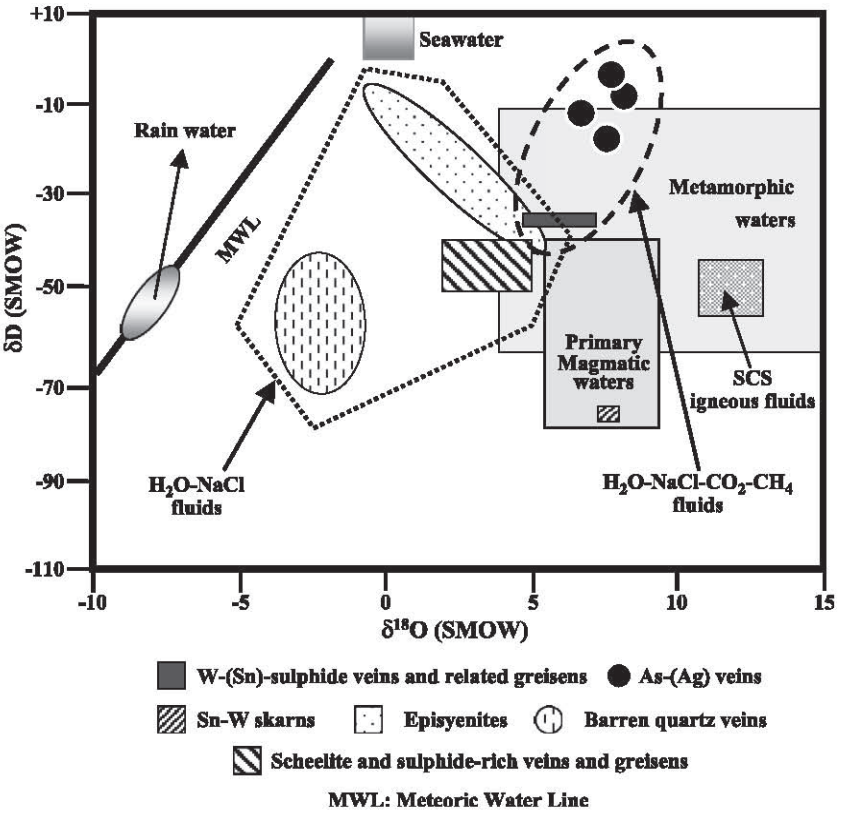

Fig. 8. Plot of $\delta^{18}O-\delta D$ values of fluids related to mineral deposits of Permian age in the Spanish Central System (SCS). The $\delta^{18}O$ and δD values are those in Table 5. Fields for the different types of waters have been taken from Sheppard (1986), and the field for the SCS igneous fluids has been taken from Tornos et al. (2000).

either directly related to a fluid exsolved from a crystallising magma or from fluids that leached magmatic rocks. If the sulphur signature was homogenised during the hydrothermal transport, a mixing of magmatic/metamorphic sources could be implied. Although no fluid inclusion data from stage II minerals are available, the stannite–sphalerite geothermometer indicates a temperature of formation for the Zn–Cu–Sn sulphide association (stage II) between 260 and 310 °C. The similar sulphur isotope composition of stage II sulphides (from 1.5‰ to 2.9‰; Table 5) to that of stage I sulphides, suggests that both mineral stages share an identical, or directly comparable sulphur source.

In contrast, the calculated $\delta^{18}O$ of water in equilibrium with stage III quartz (QII) between 170 and 230 °C ranges from −2.3‰ to +4.2‰. These values are clearly different to those related to stage I quartz precipitation and point to the presence of surficial waters (either meteoric or seawater) that interacted with the basement rocks (granitoids and low- to high-grade metamorphic rocks) during stage III of vein formation. Aqueous fluids associated with stage III are also characterised by a lower temperature and pressure than stage I. This fact, together with the isotopic composition of the fluids, shows that stage III could be disconnected from stage I, suggesting a different hydrothermal pulse. Alternatively, in the T_H/salinity plot (Fig. 6), fluid inclusion data of stage I and stage III low-salinity aqueous fluids might be also explained by a cooling process where stage III would represent the waning stages of the hydrothermal event. The lack of fluid inclusion data from stage II does not allow confirmation of any of these hypotheses. However, younger low-temperature and salinity fluids have been recognised in other mineral deposits else-

Table 6
Main geochemical characteristics of the fluids related to the Permian hydrothermal episode in the Spanish Central System and other Hercynian mineralisations

Mineralization type	Age (Ma)	Host rock	Ore assemblage	Fluid types	Bulk composition			Th (°C)	Isotopic composition		
					(mol%) H_2O	(mol%) Volatiles	(wt.%) NaCl		δS (‰)	δD (‰)	δO (‰)
W–(Sn) sulphide veins and related greisens (1)	295 ± 10	Leucogranites, orthogneisses	Cst, wf, ms, sch, asp, py, po, sl, cp, st	H_2O–NaCl–CO_2–CH_4 H_2O–NaCl	71 to 95, 91 to 97	CO_2: n.d. to 28, CH_4: n.d. to 12, N_2: n.d. to 4	0.1 to 5.1, 3 to 9	210 to 380 90 to 380	− 3.6	− 35 to − 33	4.7 to 6.9
As–(Ag) sulphide veins (this study)	286 ± 4	Orthogneisses, migmatites	Asp, py, sl, cp, po, st, gn, sfs	H_2O–NaCl–CO_2–CH_4 H_2O–NaCl	94 to 99.5, 93 to 99.5	CO_2: n.d. to 4.8, CH_4: n.d. to 4.1, N_2: n.d. to 0.2	3 to 8, 0.8 to 3.1	335 to 365 315 to 360	1.5 to 3.6	− 16 to − 2	6.4 to 8.0
Sn–W skarns (2)	284 ± 3	Granitoids	Sch, cst, asp, po, sl, cp	H_2O–NaCl	93.6 to 95.5	–	4.5 to 6.4	400 to 625	–	− 77 to − 74	7.3 to 7.8
Episyenites (3)	274 ± 6	Granitoids	Ab, px, amph, bt, ep, chl	H_2O–NaCl	93.8 to 96.4	–	3.6 to 6.2	350 to 620	–	− 45 to − 7	− 1 to 5.8
Scheelite and sulphide-rich veins and greisens (4)	267 ± 7	Leucogranites, orthogneisses	Sch, asp, cst, sl, gn, bm, st	H_2O–NaCl–KCl–($CaCl_2$–$MgCl_2$)	88.5 to 100	–	0 to 11.5	250 to 380	–	− 51 to − 40	2.1 to 4.9
Barren quartz veins (5)	274 ± 5	Granitoids, gneisses	Qtz, ms, fl	H_2O–NaCl	99 to 100	–	0 to 1	>250	–	− 75 to − 45	− 4 to 0

References: (1) Vindel et al. (1995), Tornos et al. (2000); (2) (3) (4) Tornos et al. (2000); (5) Martín Crespo et al. (2002). Ages of mineral deposits determined by K/Ar, except barren quartz veins and As–(Ag) sulphide veins determined by $^{40}Ar/^{39}Ar$. Abbreviations: ab: albite, amph: amphibole, asp: arsenopyrite, bm: bismuthinite, bt: biotite, chl: chlorite, cp: chalcopyrite, cst: cassiterite, ep: epidote, fl: fluorite, gn: galena, grt: garnet, ms: muscovite, po: pyrrhotite, px: pyroxene, py; pyrite, qtz: quartz, sch: scheelite, sfs: sulphosalts, sl: sphalerite, st: stannite, wf: wolframite. n.d.: not detected.

where in the SCS. H_2O–NaCl fluids (T_H: 120–270 °C and <3.4 wt.% NaCl eq.) identified in fluorite–barite veins (Galindo et al., 1994) have been dated as 145 Ma (Upper Jurassic), and have been related to meteoric waters. Therefore, stage III from As–(Ag) veins could also represent a post Permian hydrothermal pulse.

8.2. The Permian hydrothermal episode

The Permian age (286 ± 4 Ma.) obtained in this study for stage I As–(Ag) sulphide veins at Bustarviejo may be placed in a broader scenario. Hydrothermal episodes of Permian age have been recognised in other mineral deposits in the SCS (Table 6). These include W–(Sn) sulphide veins and related greisens, Sn–W skarns, episyenites, scheelite sulphide-rich veins and greisens, and barren quartz veins. The W–(Sn) sulphide veins are fracture-controlled, and found in the apical zones of peraluminous leucogranites and orthogneisses. The dominant component of the veins is quartz, and two ore stages can be recognised: an "oxide silicate stage" characterised by quartz, cassiterite, wolframite, muscovite, and scheelite; and a "sulphide stage" essentially characterised by the association of quartz with sulphides: arsenopyrite, pyrite, pyrrhotite, sphalerite, chalcopyrite and stannite (Noronha et al., 1999). Greisenisation and chloritisation have been clearly recognised as an extensive alteration of the granitic wallrock. Minor Sn–W skarns are formed by the replacement of marbles close to the deeper granite intrusions of the SCS. Marbles are replaced by garnet, pyroxene and idocrase, and scheelite, cassiterite, arsenopyrite, pyrrhotite, sphalerite and chalcopyrite filled later veins (Casquet and Tornos, 1984). Episyenites replace granitoids and dykes as lens-shaped bodies, and consist of albite, hedenbergite to aegirine–augite pyroxene, hastingsite amphibole, biotite, epidote and chlorite (Caballero, 1993). Scheelite sulphide-rich veins are formed by the hydrothermal reactivation of earlier W–Sn quartz veins, leading to the precipitation of scheelite, arsenopyrite, cassiterite, sphalerite, galena, bismuthinite and stannite. Cassiterite–scheelite sulphide-bearing chlorite-rich greisens are also formed in the contact with the wallrock (Tornos et al., 1993). A large number of barren quartz veins have been identified throughout the granitic and metamorphic outcrops of the SCS. Two main morphological and textural types of quartz are distinguished, massive quartz at the vein margins and clear quartz crystals in the centre of the veins. Hydrothermal muscovite and minor amounts of fluorite and Fe oxides have been recognised located between quartz crystals. Hydrothermal alteration is poorly developed and restricted to the proximity of the lodes. Replacement of feldspars by muscovite and chloritisation of biotite within the granites are the usual and most important types of alteration (Martín Crespo et al., 2002).

Two types of fluids have been distinguished in relation to these hydrothermal events (Vindel et al., 1995; Tornos et al., 2000; Martín Crespo et al., 2002): (i) aqueous–carbonic fluids related to 300–280 Ma (Early Permian) W–(Sn) sulphide veins, and (ii) 280–260 Ma (Late Permian) aqueous fluids, associated to episyenites, barren quartz veins and scheelite sulphide-rich veins and related greisens. The Sn–W skarns, which are also characterised by the presence of aqueous fluids, would be related to the Early Permian event (284 ± 3 Ma).

Fluids related to the Early Permian event are characterised by the presence of significant amounts of CO_2 and CH_4 with minor N_2. In a $\delta^{18}O$–δD diagram (Fig. 8), those deposits associated with aqueous–carbonic fluids plot in an area defined by metamorphic waters. In accordance to the $\delta^{18}O$–δD data, the sulphur isotope composition of sulphides associated with this event, points to an origin related to magmatic and/or metamorphic rocks. Although these deposits are both spatially and temporally associated to granitic intrusions, the proportion of magmatic fluids involved in the hydrothermal activity of the SCS has been considered as minor because of the water-undersaturated character of the intrusions. The presence of CH_4 indicates that fluid chemistry of W–(Sn) sulphide veins was controlled by graphite–fluid equilibrium, implying a source for fluids external to the granite such as the surrounding metamorphic rocks (Vindel et al., 1995).

The Late Permian hydrothermal event (280–60 Ma.) is characterised by H_2O–NaCl undersaturated fluids of low to moderate salinity (0–11.5 wt.% NaCl eq.) and has been recognised as the main fluid input in the development of episyenites, barren quartz veins and scheelite–sulphide-rich veins and greisens. $\delta^{18}O$ and δD isotope values plot outside the

metamorphic and magmatic water fields, suggesting the involvement of meteoric waters that underwent variable water/rock interaction (Fig. 8). In this late event, two main groups can be distinguished on the basis of their isotopic signature: (i) episyenites and scheelite sulphide-rich veins, and (ii) barren quartz veins. The first type of hydrothermal deposits record a wide range of the $\delta^{18}O$ of the fluids, from slightly negative to positive values ($-1‰$ to $+5.8‰$), and waters related to the formation of barren quartz veins show low $\delta^{18}O$ ($-4‰$ to $0‰$) and extremely low δD (-75 to $-45‰$) values. The isotope composition and the low salinity of the fluids involved in the origin of deposits from the first group suggest that they were modified meteoric waters (Caballero, 1993; Tornos et al., 2000). The more $\delta^{18}O$-enriched values can be explained as resulting from fluid equilibration at low fluid/rock ratios with granites or gneisses, whereas the less $\delta^{18}O$-enriched values indicate more fluid dominated systems emphasizing the importance of fluid/rock interactions. The low (<1 wt.% NaCl eq.) salinity, the moderate temperature and the isotopic composition of the H_2O–NaCl fluids involved in the genesis of the barren quartz veins indicate a meteoric origin for water, with significant water/rock interactions (Martín Crespo et al., 2002). Fluids related to barren quartz veins show more negative $\delta^{18}O$ values than fluids related to episyenites and to scheelite sulphide-rich veins because of the exclusive meteoric origin of waters involved in their genesis.

The age and composition of fluids associated to ore stage I (As–Fe) at Bustarviejo allow us to tentatively assign this mineralising stage to the older Permian hydrothermal event (Table 6). The carbonic fluids associated to the As–Fe event show similar salinity and T_H ranges than fluids related to W ores, but lower CO_2, CH_4 and N_2 contents. The O, H and S isotopic signature of stage I fluids would not necessarily be related to a magmatic event but derived from hydrothermal leaching of igneous rocks (granites and orthogneisses) at temperatures around 360 °C in relation to hydrothermal cells at the roof zones of small granitic intrusions (Tornos et al., 2000). The dominant mechanism of sulphide deposition for stage I (As–Fe) could be a mixing process between aqueous–carbonic (Lw-c) and aqueous (Lw1) fluids, and cooling processes between aqueous (Lw2) and hypersaline (Lw-s) fluids characterize the stage III (Pb–Ag). Therefore, the similar composition and evolution of the aqueous–carbonic fluids seem to suggest a common origin for W–(Sn) sulphide veins and Bustarviejo stage I mineralisations. These aqueous–carbonic fluids would result from waters isotopically equilibrated with metamorphic rocks with later inputs of aqueous ($NaCl–H_2O$) fluids. Dilution and cooling characterise the whole evolution of volatile-rich fluid stages (stage I and possibly stage II at Bustarviejo), although evidence for a later fluid input, probably not related to the main depositional stage, is given by the presence of waters of surficial origin. Based on observed geological relationships, age, composition of involved fluids and isotope signature, As–(Ag) sulphide veins (main stages: I and II) are comparable to W–(Sn) sulphide veins. Both are located in the same geological scenario, are dated around 290 Ma, aqueous–carbonic fluids are involved in their formation, and show similar $\delta^{18}O$ and δD signatures, leading to a origin related to waters isotopically equilibrated with metamorphic or igneous rocks.

The structural setting and the mineralogical, isotopic and fluid inclusion signature of the major hydrothermal events in the SCS are clearly different. The evolution of Permian fluids is characterised by dilution and cooling processes, from early C–H–O–N fluids controlled by water–rock interactions to late H_2O–NaCl fluids dominated by the presence of meteoric waters. External waters of metamorphic and meteoric signature penetrated into shallow granite intrusions, channelled by minor faults. Water/rock reaction was the most important process causing changes in the isotopic composition of fluids prior to fluid mixing at shallow depths. The transition from these spatially confined systems to regional-scale systems occurred at about 275 Ma (beginning of the Alpine cycle), when the morphology and chemistry of these hydrothermal systems changed drastically. A generalised percolation of meteoric fluids (H_2O–NaCl) within the crust, defining major convective cells dominated by regional extensional faults has been demonstrated (Tornos et al., 2000). H_2O–NaCl fluids have also been recognised in the early Permian deposits (300–280 Ma) because of the extensional pulses at the start of the Alpine orogeny in the SCS (González Casado et al., 1996), allowing the penetra-

tion of meteoric fluids into the crust, which were subsequently heated, and reacted with igneous and metamorphic rocks. Therefore, this type of fluid is the result of a major hydrothermal circulation event, coincident with the Mid-Permian transition to extensional pre-rift tectonics, and is ubiquitous throughout the SCS.

9. Conclusions

As–(Ag) sulphide veins at Bustarviejo record a detailed evolution of the hydrothermal activity that took place during the Permian in the Spanish Central System. The veins are characterised by multistage ore deposition developed along three hydrothermal stages: (I) As–Fe stage, (II) Zn–Cu–Sn stage and (III) Pb–Ag–Bi stage, followed by late supergene alteration processes (stage IV).

Fluid inclusion and stable isotope (O, D and S) data indicate the presence of two major types of fluids in the hydrothermal system: an aqueous–carbonic fluid related to stage I, and an aqueous fluid related to stages I and III. The fluid evolution during ore stage I (>350 °C; >0.3 kbar) has been interpreted as resulting from an isothermal mixing process, where fluids, equilibrated at relatively high temperature, are progressively diluted by aqueous fluids. Deposition of arsenopyrite, pyrite and other minerals from stage I could be interpreted as result of this mixing process. The presence of stannite in equilibrium with sphalerite indicates a temperature deposition of 275 ± 25 °C for stage II sulphides. Stage III is characterised by the presence of low-temperature (200 ± 30 °C), low-salinity (< 2% NaCl wt.% eq.) and low-pressure (< 0.5 kbar) aqueous fluids, probably representing a later hydrothermal event, not related to the previous stages. In any case, the isotopic signature of these late fluids indicates that this hydrothermal pulse was dominated by meteoric waters. It is likely that a temperature drop could cause the precipitation of minerals in stage III.

The age (^{40}Ar–^{39}Ar) of the As–Fe stage (I) in the sulphide veins, determined on coeval muscovite is 284 ± 4 Ma, which allows to include this mineralisation within the Permian hydrothermal episode of the SCS.

Similar features characterise other mineral deposits of Permian age in the SCS, in which two main hydrothermal episodes had been identified. The early (300–280 Ma) hydrothermal event is represented by relatively high temperature aqueous–carbonic and aqueous fluids heated and reacted with the surrounding rocks, and is represented by W–(Sn) sulphide veins and related greisens and As–(Ag) sulphide veins. The late (280–260 Ma) hydrothermal event is characterised by meteoric aqueous fluids, and represented by episyenites, scheelite sulphide-rich veins and greisens and barren quartz veins. The transition between both events occurs around 275 Ma, at the beginning of the Alpine cycle, coincident with the Mid-Permian transition to extensional pre-rift tectonics, when late aqueous fluids circulated under a low-pressure regime.

Acknowledgements

M.C. Boiron (CREGU-G2R, Nancy France) and I. Villa (Bern University, Switzerland) are thanked for their comments and technical support with Raman and geochronology analysis, respectively. The authors thank the editor N.J. Cook and the two anonymous reviewers for their helpful comments. Financial support for this work has been provided by the Universidad Complutense de Madrid, via project PR78/02-11047.

References

Amorós, J.L., López, J.A., Lunar, R., Martínez, J., Sierra, J., Vindel, E., 1984. Chalcopyrite–sphalerite textures in some Spanish syngenetic and epigenetic deposits: Guadarrama Mountains, Aznalcollar and La Union. In: Wauschkuhn, A., Kluth, C., Zimmermann, R.A. (Eds.), Syngenesis and Epigenesis in the Formation of Mineral Deposits. Springer-Verlag, Berlin, pp. 18–27.

Bakker, R.J., 1999. Adaptation of the Bowers and Helgeson (1983) equation of state to the H_2O–CO_2–CH_4–N_2–NaCl system. Chemical Geology 154, 225–236.

Bakker, R.J., Dubessy, J., Cathelineau, M., 1996. Improvements in clathrate modelling: I. The H_2O–CO_2 system with various salts. Geochimica et Cosmochimica Acta 60, 1657–1681.

Bodnar, R.J., 1993. Revised equation and table for determining the freezing point depression of H_2O–NaCl solutions. Geochimica et Cosmochimica Acta 57, 683–684.

Boiron, M.-C., Essarraj, S., Sellier, E., Cathelineau, M., Lespinasse, M., Poty, B., 1992. Identification of fluid inclusions in relation to their host microstructural domains in quartz by cathodoluminescence. Geochimica et Cosmochimica Acta 56, 175–185.

Caballero, J.M., 1993. Las episienitas de la Sierra de Guadarrama: un caso singular de alteración hidrotermal de edad post-hercínica. Unpublished PhD thesis. Universidad Complutense, Madrid. 313 pp.

Caballero, J.M., Casquet, C., Galindo, C., González-Casado, J.M., Snelling, N., Tornos, F., 1992. Dating of hydrothermal events in the Sierra de Guadarrama, Iberian Hercynian Belt, Spain. Geogaceta 11, 18–22.

Casquet, C., Tornos, F., 1984. El skarn de W–Sn del Carro del Diablo (Sistema Central Español). Boletín Geológico y Minero 95, 58–78.

Casquet, C., Fúster, J.M., González Casado, J.M., Peinado, M., Villaseca, C., 1988. Extensional tectonics and granite emplacement in the Spanish Central System. A discussion. In: Banda, L.A., Mendes-Víctor, L.A. (Eds.), V EGT Workshop: The Iberian Peninsula. European Science Foundation, Strasbourgh, France, pp. 65–77.

Clayton, R.N., Mayeda, T.K., 1963. The use of bromine pentafluoride in the extraction of oxygen from oxides and silicates for isotopic analysis. Geochimica et Cosmochimica Acta 27, 43–52.

Doblas, M., Oyarzun, R., Sopeña, A., López Ruiz, J., Capote, R., Hernández Enrile, J.L., Lunar, R., Sánchez, Y., 1994. Variscan–late Variscan–early Alpine progressive extensional collapse of central Spain. Geodinámica Acta 7, 1–14.

Escuder, J., Hernáiz, P.P., Valverde-Vaquero, R., Rodríguez, R., Dunning, G., 1998. Variscan syncollisional extension in the Iberian Massif: structural, metamorphic and geochronological evidence from the Somosierra sector of the Sierra de Guadarrama (Central Iberian Zone, Spain). Tectonophysics 290, 87–109.

Foord, E.E., Shawe, D.R., 1989. The Pb–Bi–Ag–Cu–(Hg) chemistry of galena and some associated sulphosalts: a review and some new data from Colorado, California and Pennsylvania. Canadian Mineralogist 27, 363–382.

Galindo, C., Tornos, F., Darbyshire, D.P.F., Casquet, C., 1994. The age and origin of the barite–fluorite (Pb–Zn) veins of the Sierra de Guadarrama (Spanish Central System, Spain): a radiogenic (Nd, Sr) and stable isotope study. Chemical Geology 112, 351–364.

González Casado, J.M., Caballero, J.M., Casquet, C., Galindo, C., Tornos, F., 1996. The transition Hercynian–Alpine cycle in the Sierra de Guadarrama (Eastern Iberian Central System). Paleostress field and geotectonic interpretation. Tectonophysics 262, 213–229.

González Laguna, R., Lozano, R., Casquet, C., 2000. Efectos de alteración hidrotermal en los minerales accesorios del granito de La Cabrera (Sistema Central Español). Estudio al microscopio electrónico de barrido (SEM+EDS). Boletín Sociedad Española de Mineralogía 23, 135–148.

Kamber, B.S., Blenkinsop, T.G., Villa, I.M., Dahl, P.S., 1995. Proterozoic transpressive deformation in the Northern Marginal Zone, Limpopo Belt, Zimbawe. Journal of Geology 103, 493–508.

Lozano, R., Casquet, C., González Laguna, R., 1999. Bolsadas pegmatíticas con cavidades rellenas de minerales hidrotermales en el plutón de La Cabrera (Sistema Central Español). Modelo de evolución. Boletín Sociedad Española de Mineralogía 22-A, 63–64.

Martín Crespo, T., López García, J.A., Banks, D., Vindel, E., García, E., 1999. Hydrothermal fluids in barren quartz veins (Spanish Central System). A comparison with W (Sn) and F (Ba) veins. Boletín Sociedad Española de Mineralogía 22, 83–94.

Martín Crespo, T., Delgado, A., Vindel, E., López García, J.A., Fabre, C., 2002. The latest Post-Variscan fluids in the Spanish Central System: evidence from fluid inclusion and stable isotope data. Marine and Petroleum Geology 19, 323–337.

Martinez Frías, J., Vindel, E., Lunar, R., 1984. Estudio textural y metalogénico de la mineralización de Bustarviejo (Sierra de Guadarrama), Materiales y Procesos. Facultad Ciencias Geológicas, Universidad Complutense 2, 68–75.

Nagase, T., Kojima, S., 1997. An SEM examination of the chalcopyrite disease texture and its genetic implications. Mineralogical Magazine 61, 89–97.

Nakamura, Y., Shima, H., 1982. Fe and Zn partitioning between sphalerite and stannite. Joint Meeting of the Society of Mining Geologists of Japan, Japanese Association of Mineralogists, Petrologists and Economic Geologists, and Mineralogical Society of Japan, A-8. In Japanese.

Noronha, F., Dória, A., Nogueira, P., Boiron, M.C., Cathelineau, M., 1995. A comparative study of the fluid evolution in late-Hercynian W–(Sn–Cu) and Au (As) quartz veins in Northern Portugal. Metallogenic implications. IV Congresso Nacional de Geologia. Resumos alargados. Memoria do Museu e Laboratório Mineralógico e Geológico da Faculdade de Ciencias do Porto, vol. 4, pp. 587–592.

Noronha, F., Vindel, E., López, J.A., Dória, A., García, E., Boiron, M.C., Cathelineau, M., 1999. Fluids related to tungsten ore deposits in northern Portugal and Spanish Central System: a comparative study. Revista Sociedad Geológica de España 12, 397–403.

Ramdohr, P., 1969. The Ore Minerals and their Intergrowths, English edition. Pergamon, Oxford. 1174 pp.

Samper, J., 1977. Estudio metalogénico y evolución de la minería en la mina Mónica de Bustarviejo. Tecniterrae 19, 14–22.

Sheppard, S.M.F., 1986. Characterization and isotopic variations in natural waters. In: Valley, J.W., Taylor, H.P., O'Neil, J.R. (Eds.), Stable Isotopes in High Temperature Geological Processes. Reviews in Mineralogy, vol. 16, pp. 165–183.

Suzuoki, T., Epstein, S., 1976. Hydrogen isotope fractionation between OH-bearing minerals and water. Geochimica et Cosmochimica Acta 40, 1229–1240.

Thiery, R., Vidal, J., Dubessy, J., 1994. Phase equilibria modelling applied to fluid inclusions liquid–vapour equilibria and calculation of the molar volume in the CO_2–CH_4–N_2 system. Geochimica et Cosmochimica Acta 58, 1073–1082.

Tornos, F., Casquet, C., Caballero, J.M., 1993. La alteración hidrotermal asociada al plutón epizonal de Navalcubilla, Sierra de Guadarrama (Sistema Central Español). Revista Sociedad Geológica de España 6, 67–84.

Tornos, F., Delgado, A., Casquet, C., Galindo, C., 2000. 300 million years of episodic hydrothermal activity: stable isotope ev-

idence from hydrothermal rocks of the Eastern Iberian Central System. Mineralium Deposita 35, 551–569.

Vialette, Y., Bellido, F., Fúster, J.M., Ibarrola, E., 1981. Datos geocronológicos sobre el granito de La Cabrera. Cuadernos Geología Ibérica 7, 327–338.

Vialette, Y., Casquet, C., Fúster, F., Ibarrola, J.M., Navidad, E., Peinado, M., Villaseca, M., 1987. Geochronological study of orthogneisses from the Sierra de Guadarrama (Spanish Central System). Neues Jahrbuch für Mineralogie, Monatshefte 10, 465–479.

Villa, I.M., 1998. Isotopic closure. Terra Nova 10, 42–47.

Villaseca, C., Herreros, V., 2000. A sustained felsic magmatic system: the Hercynian granitic batholith of the Spanish Central System. Transactions of the Royal Society of Edinburgh, Earth Sciences 91, 207–219.

Villaseca, C., Eugercios, L., Snelling, N.J., Huertas, M.J., Castellón, T., 1995. Nuevos datos geocronológicos (Rb–Sr, K–Ar) de granitoides hercínicos de la Sierra de Guadarrama. Revista Sociedad Geológica de España 8, 129–140.

Villaseca, C., Barbero, L., Rodgers, G., 1998. Crustal origin of Hercynian peraluminous granitic batholiths of Central Spain: petrological, geochemical and isotopic (Sr, Nd) constraints. Lithos 43, 55–79.

Vindel, E., 1980. Estudio mineralógico y petrológico de las mineralizaciones de la Sierra de Guadarrama. Unpublished PhD thesis, Complutense Univ. Madrid. 249 pp.

Vindel, E., Lopez, J.A., Boiron, M.C., Cathelineau, M., Prieto, A.C., 1995. $P–V–T–X–fO_2$ evolution from wolframite to sulphide depositional stages in intragranitic W-veins. An example from the Spanish Central System. European Journal of Mineralogy 7, 655–673.

Vindel, E., Lopez, J.A., Martín Crespo, T., García, E., 2000. Fluid evolution and hydrothermal processes of the Spanish Central System. Journal of Geochemical Exploration 69–70, 359–362.

Zhang, Y., Frantz, D., 1987. Determination of the homogenisation temperatures and densities of supercritical fluids in the system $NaCl–KCl–CaCl_2–H_2O$ using synthetic fluid inclusions. Chemical Geology 64, 335–350.

Zheng, Y.F., 1993. Calculation of oxygen isotope fractionation in hydroxyl-bearing silicates. Earth and Planetary Science Letters 120, 247–263.